

# Nodal line semimetals through boundary

Protyush Nandi<sup>1,\*</sup> and Subinay Dasgupta<sup>2,†</sup>

<sup>1</sup>*Department of Physics, University of Calcutta, 92 Acharya Prafulla Chandra Road, Kolkata 700009, India*

<sup>2</sup>*Department of Physics, Harish-Chandra Research Institute, Prayagraj 211019, India*

We study the properties of a spinless Hamiltonian which describes topological nodal line semimetals at zero temperature. Our Hamiltonian has some resemblance with the usual Hamiltonian for this type of materials, with that of Weyl semimetals and is some sort of a generalisation of Kitaev Hamiltonian on honeycomb lattice. As the interaction parameter of the Hamiltonian is varied, it shows a transition from a gapless phase to a semimetal phase and then to another semimetal phase. These transitions show up as non-analytic behaviour of ground state energy. We find that one type of the semimetal is characterised by a single closed loop of nodal line, while the other, by two such loops both crossing the boundary of the first Brillouin zone. Surface states with non-zero winding number are found to exist in both of these phases, but over two topologically different regions. We also study the length of nodal line, the area and perimeter of the region over which the winding number is non-zero and the low-frequency electrical conductivity.

**Introduction:** Among the different types of topological materials, topological nodal line semimetals (TNLSM) have a unique importance due to their distinctive properties, like flat drumhead states [19–21], graphene like transport properties in 3D [1] and surface superconductivity possibly at high temperatures [18]. These materials also show unique plasmon mode behaviour [23, 24] and flat Landau levels at Fermi levels which are unusual in 3D materials.[22]. Long range Coulomb interaction in nodal line semimetals has also been reported [25]. It also shows anomalous Andreev reflection and both 3D and 2D weak anti-localization effects that can be probed by magnetoconductivity [26]. These materials are characterised by the presence of nodal points (where the conduction and valence bands touch) along a closed loop near the Fermi surface in the momentum space. Usually they are described by a  $2 \times 2$  Hamiltonian

$$\mathcal{H}_{\vec{k}}^0 = vk_z\sigma_x + (k^2 - k_0^2)\sigma_z \quad (1)$$

in the space of wavevectors  $\vec{k}$ . (Here  $v$  and  $k_0$  are the parameters of the model and  $\sigma_z, \sigma_x$  stand for Pauli matrices.) This Hamiltonian shows an insulator to semimetal transition as the parameter  $k_0$  is varied. Various materials have been identified as potential candidates for TNLSM [26]. Some years back it was discovered that PbTaSe<sub>2</sub> having nodal lines, is superconducting below 3.8K [5]. It seems important to study various types of Hamiltonian that gives rise to nodal lines.

In this short communication, we consider a  $2 \times 2$  spinless Hamiltonian

$$\mathcal{H} = \sum_{\vec{k}} \mathcal{H}_{\vec{k}}, \quad \mathcal{H}_{\vec{k}} = A_{\vec{k}}\sigma_z + B_{\vec{k}}\sigma_x \quad (2)$$

with

$$A_{\vec{k}} = J - \cos k_x - \cos k_y - \cos k_z \quad B_{\vec{k}} = \sin k_x + \sin k_y + \sin k_z \quad (3)$$

where,  $J$  is a parameter and  $\vec{k}$  runs over the first Brillouin zone of a cubic lattice  $-\pi < k_x, k_y, k_z \leq \pi$ . As  $J$  is decreased from above a value 3, this Hamiltonian shows a transition at  $J = 3$  from an insulator phase (no nodal point) to a semimetal phase (one closed nodal loop lying within the first Brillouin zone) and then at  $J = 1$  to a second semimetal phase (with two nodal loops crossing the Brillouin zone boundary). This second transition has not been reported till now, to our knowledge. A similar transition, however, is known to occur in Weyl semimetals [12] where the transition occurs from a phase with one pair of nodal points to a phase with two pairs of nodal points. Also, a similar type of nodal lines has been reported for Weyl nodal lines [6].

We shall first present motivation for our Hamiltonian and then discuss its various properties. We shall not attempt to guess what type of real material might be represented by this Hamiltonian.

**Motivation:** (1) On the plane  $k_x = -k_y$ , for small  $\vec{k}$ , our Hamiltonian of Eq. (2) reduces to the usual Hamiltonian of Eq. (1) upto terms quadratic in  $\vec{k}$ .

(2) The usual Hamiltonian for Weyl semimetal [2, 3, 7, 8]

$$\mathcal{H}_{\vec{k}}^W = (J - \cos k_x - \cos k_y - \cos k_z)\sigma_z + \sin k_x\sigma_x + \sin k_y\sigma_y \quad (4)$$

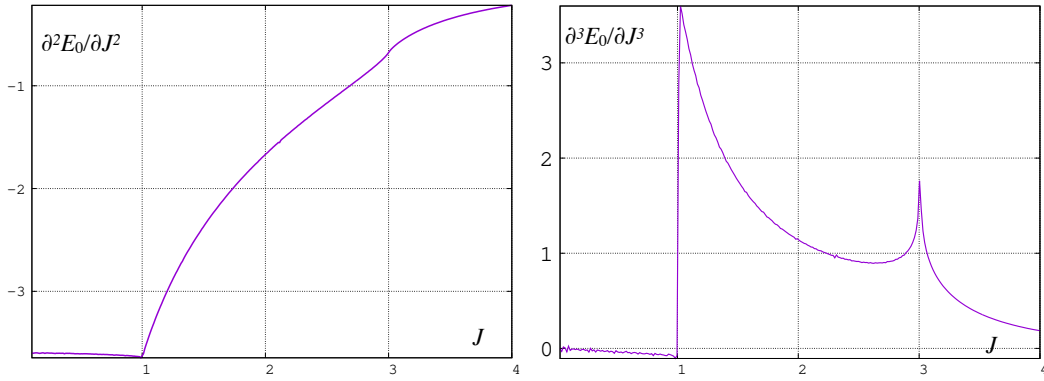


FIG. 1. Derivatives of ground state energy calculated from Eq. (6) for  $N = 300^3$ .

has a form similar to Eq. (2).

(3) Kitaev model on honeycomb lattice can be represented [7, 8] by Eq. (2) with

$$A_{\vec{k}} = J - \cos k_x - \cos k_y \quad B_{\vec{k}} = \sin k_x + \sin k_y$$

and a straightforward generalisation of these equations lead to Eq. (3).

**Ground State Energy:** The ground state energy (per site) is

$$E_0 = \frac{1}{N} \sum_{\vec{k}} \lambda_{\vec{k}} \quad (5)$$

where  $N$  is the total number of sites and  $\lambda_{\vec{k}} = \sqrt{A_{\vec{k}}^2 + B_{\vec{k}}^2}$ . The second derivative of this quantity, namely,

$$\frac{\partial^2 E_0}{\partial J^2} = \frac{1}{N} \sum_{\vec{k}} \frac{B_{\vec{k}}^2}{\lambda_{\vec{k}}^3} \quad (6)$$

when plotted against  $J$ , shows a prominent kink at  $J = 1$  and a less prominent one at  $J = 3$  (Fig. 1). However, such kinks are not visible in the curves  $E_0$  vs  $J$  and  $\partial E_0/\partial J$ .

One may be curious to check if the new transition at  $J = 1$  comes also from the usual Hamiltonian of Eq. (1). However, since this Hamiltonian is typically suited for small values of  $k$ , we make the replacements

$$vk_z \rightarrow 2 \sin k_z \quad k^2 \rightarrow 2(3 - \cos k_x - \cos k_y - \cos k_z) \quad 3 - k_0^2 \rightarrow J \quad (7)$$

following Shen [9] and arrive at the Hamiltonian

$$\mathcal{H}_{\vec{k}}^1 = \sin k_z \sigma_x + (J - \cos k_x - \cos k_y - \cos k_z) \sigma_z \quad (8)$$

The two transitions at  $J = 1, 3$  are observed in the ground state energy vs  $J$  curve for this Hamiltonian also (Fig. 3). However, if we make *only* the substitution  $3 - k_0^2 \rightarrow J$  and study the Hamiltonian of Eq. (1) as a function of  $J$  then we shall miss the transition at  $J = 1$ .

**Nodal Lines:** These lines consist of the points which satisfy  $A_{\vec{k}} = 0$  and  $B_{\vec{k}} = 0$ , with  $A_{\vec{k}}, B_{\vec{k}}$  given by Eq. (3). For a given  $k_z$ , one obtains,

$$2 \cos \frac{k_x + k_y}{2} \cos \frac{k_x - k_y}{2} = J - \cos k_z \quad 2 \sin \frac{k_x + k_y}{2} \cos \frac{k_x - k_y}{2} = -\sin k_z. \quad (9)$$

and one can solve out  $k_x, k_y$  from here. The geometry of the nodal lines for different values of  $J$  are shown in Fig. 3 and Fig. 4. For  $1 < J < 3$  there is one closed line of nodal points and this line lies entirely within the Brillouin zone. For  $J < 1$  the nodal points lie on two closed lines, each of which crosses the boundary of the zone and reappears from the opposite side in view of the periodic boundary condition.

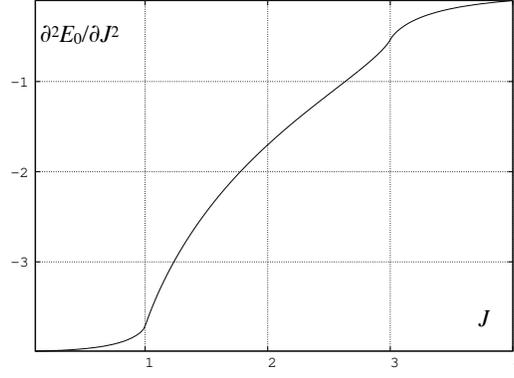


FIG. 2. Derivatives of ground state energy calculated from Eq. (8) for  $N = 300^3$ .

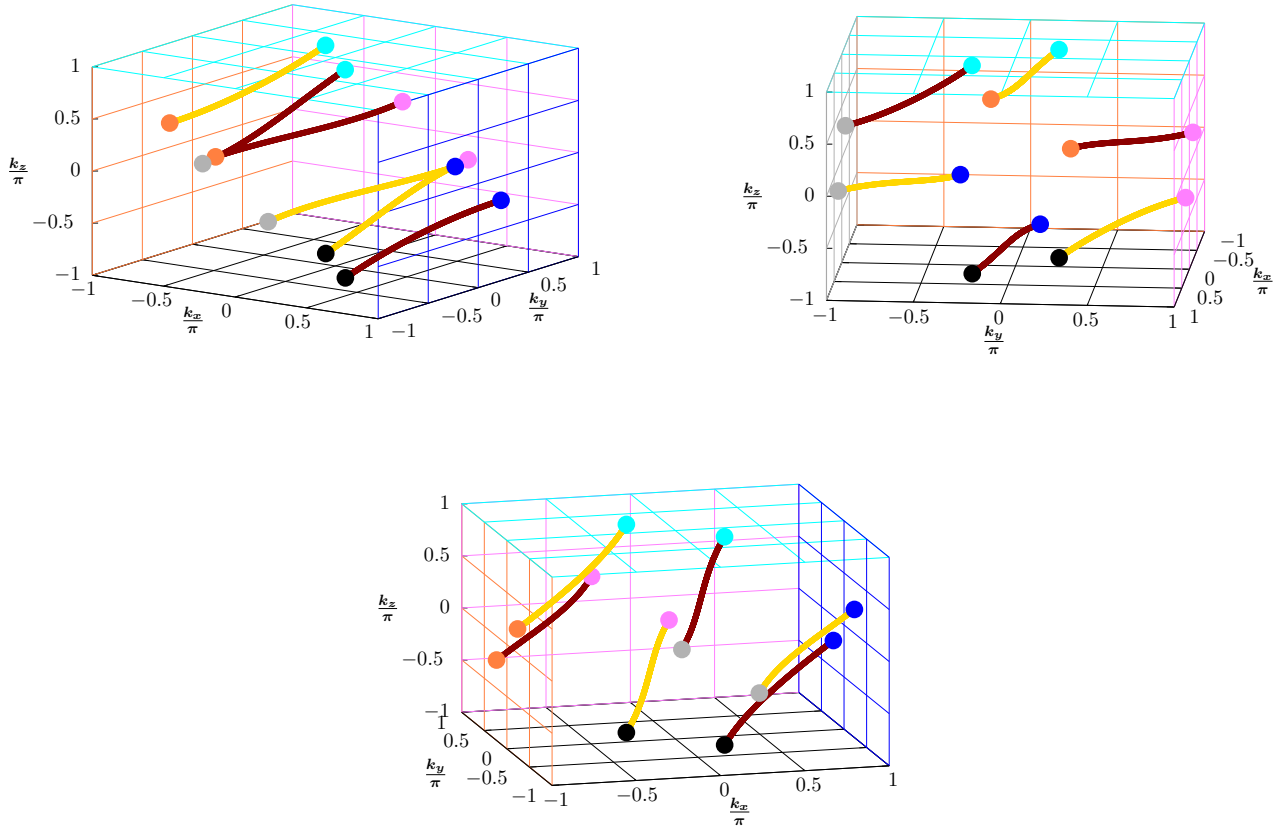


FIG. 3. The nodal line structure for  $J = 0.5$  is shown. The colored balls signify the points where the nodal lines meet the boundary surfaces. We can see that the yellow lines and the dark red lines are in fact two nodal lines joined by the periodic boundaries of the Brillouin zone.

**Time Reversal Symmetry:** The time reversal operator is

$$\mathcal{T} = \mathbf{1}\mathcal{K} \quad (10)$$

where  $\mathcal{K}$  is complex conjugation operator [10, 11] and we observe,

$$\mathcal{T}\mathcal{H}_{\vec{k}}\mathcal{T}^{-1} = \mathcal{H}_{-\vec{k}} = A_{-\vec{k}}\sigma_z + B_{-\vec{k}}\sigma_x = A_{\vec{k}}\sigma_z - B_{\vec{k}}\sigma_x \quad \mathcal{T}(A_{\vec{k}}\sigma_z + B_{\vec{k}}\sigma_x)\mathcal{T}^{-1} = A_{\vec{k}}\sigma_z + B_{\vec{k}}\sigma_x \quad (11)$$

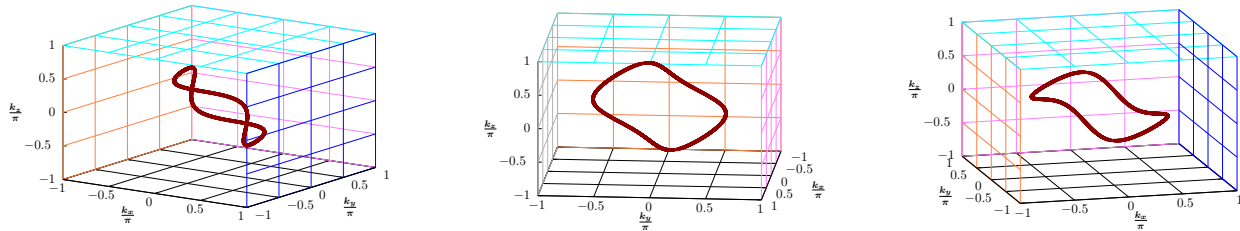


FIG. 4. The nodal line structure for  $J = 1.5$  is shown here. The dark red line is a single nodal ring within the Brillouin zone and does not touch any boundary surface.

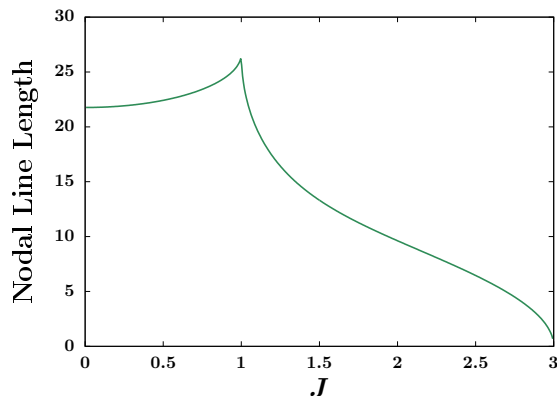


FIG. 5. The length of the nodal line is plotted w.r.t  $J$  for  $N = 2000^3$

Since the Brillouin zone is symmetric about  $\vec{k} = 0$ , corresponding to every  $\vec{k}$  in the sum of Eq. (2) there will be a  $-\vec{k}$ . Hence our Hamiltonian is time-reversal symmetric. If we construct  $\mathcal{H}_{\vec{k}}$  as  $A_{\vec{k}}\sigma_z + B_{\vec{k}}\sigma_y$  then also it will be time-reversal symmetric. By the same argument, the Hamiltonian is also invariant under inversion symmetry.

**Length of Nodal Lines:** The length of nodal, computed numerically, shows a peak at  $J = 1$  (Figure). For the special case of  $J = 1$ , one obtains a simple expression for the nodal lines,

$$(k_x, k_y, k_z) = (0, \pi + k_z, k_z) \quad \text{for } -\pi < k_z < 0$$

and permutations thereof. This gives the length of nodal line as  $6\sqrt{2}\pi$ . As  $J$  decreases below 1, the length saturates to a value  $\approx 22$ .

**Winding Number:** We write the Hamiltonian  $\mathcal{H}_{\vec{k}}$  of Eq. (2) as

$$\mathcal{H}_{\vec{k}} = R_x\sigma_z + R_y\sigma_x \quad (12)$$

where we introduce a vector  $\vec{R}$  with components

$$R_x = J - \cos k_x - \cos k_y - \cos k_z, \quad R_y = \sin k_x + \sin k_y + \sin k_z \quad (13)$$

Let us recall the method of calculation of winding number for SSH model, where one can write the Hamiltonian in the form of Eq. (12), but with a scalar wave vector. One then runs the wave vector across the Brillouin zone and checks if the tip of the vector  $\vec{R}$  makes a round about the origin. In 3D, scanning the Brillouin zone will be complicated and hence, following [1] we scan the component  $k_z$  for every value of  $(k_x, k_y)$ . This will lead to some sort of a uniaxial winding number. We note that

$$(R_x - x_0)^2 + (R_y - y_0)^2 = 1, \quad \text{with } x_0 = J - \cos k_x - \cos k_y, \quad y_0 = \sin k_x + \sin k_y \quad (14)$$

which implies that the tip of the vector  $\vec{R}$  moves over a circle with radius 1 and centre  $(x_0, y_0)$ . Therefore, the winding number  $W$  will be 1 or 0 according as  $x_0^2 + y_0^2$  is smaller or larger than 1 respectively. The regions for two values of

$J$  are shown in Fig. 5. One finds that for  $1 < J < 3$ , the  $W = 1$  points form a patch around the origin, while for  $J < 1$ , in view of the periodic boundary conditions, the  $W = 1$  points form a ring. Thus, as  $J$  crosses the value 1 from above, the region of  $W = 1$  points change from a simply connected region to a multiply connected one.

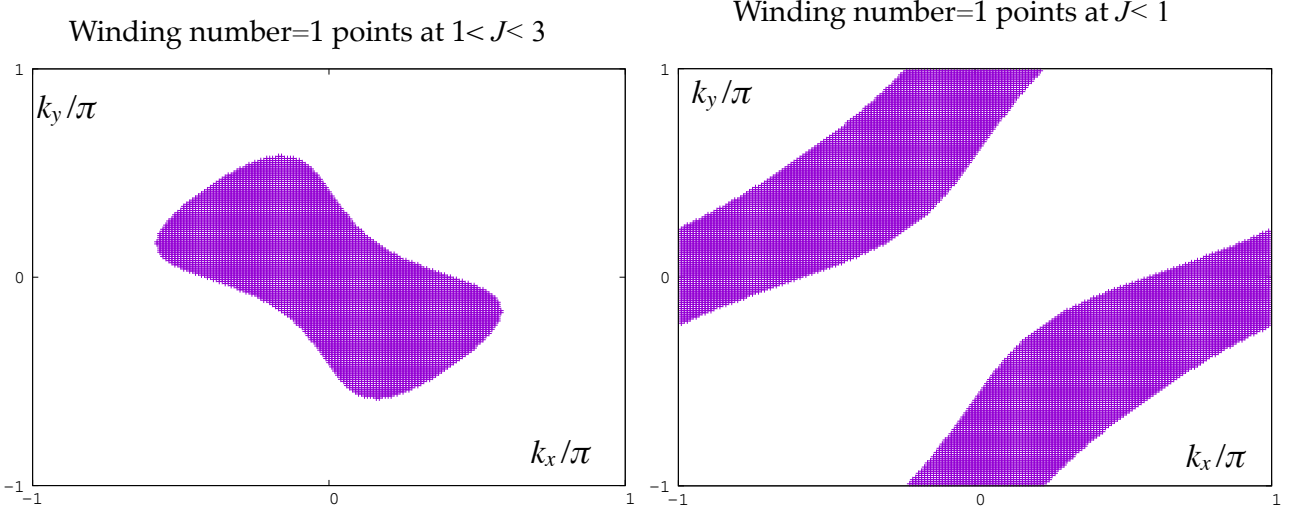


FIG. 6. Region of winding number 1 is marked for  $J = 1.5$  (left figure) and  $J = 0.5$  (right figure)

**Surface States:** We write the full Hamiltonian of the system as

$$\mathcal{H}_f = \sum_{\vec{k}} c_{\vec{k}}^\dagger \mathcal{H}_{\vec{k}} c_{\vec{k}} \quad (15)$$

where  $c_{\vec{k}}^\dagger = (c_{\vec{k}A}^\dagger \ c_{\vec{k}B}^\dagger)$  and  $\vec{k} = (k_x \ k_y \ k_z)$ . By (inverse) Fourier transformation [2] in the  $z$  direction, one can switch over to  $c_{k_x k_y n_z}$  and get

$$\mathcal{H}_f = \sum_{k_x, k_y, n_z} \left[ c_{k_x k_y n_z}^\dagger (\Delta_1 \sigma_z + \Delta_2 \sigma_x) c_{k_x k_y n_z} + c_{k_x k_y n_z}^\dagger \left( -\frac{1}{2} \sigma_z - \frac{i}{2} \sigma_x \right) c_{k_x k_y n_z + 1} + c_{k_x k_y n_z + 1}^\dagger \left( -\frac{1}{2} \sigma_z + \frac{i}{2} \sigma_x \right) c_{k_x k_y n_z} \right] \quad (16)$$

where  $\Delta_1 = J - \cos(k_x) - \cos(k_y)$  and  $\Delta_2 = \sin(k_x) + \sin(k_y)$ . From this equation we have calculated numerically the number of states having zero energy with  $n_z$  lying in the upper or lower surface of the sample. The result (Fig. 9) is that the number of zero energy states is higher on the surface than in the bulk and that the number of surface states is higher for  $J < 1$  phase. Surface states will exist for only those values of  $(k_x, k_y)$  for which  $\Delta_1^2 + \Delta_2^2 \leq 1$ . This region is marked in Fig. (6) as the one where the winding number is 1. In fact the area and perimeter of this region also shows non-analyticity at  $J = 1$  and 3.

**Conductivity:** The expression for optical conductivity for TNLSM has been studied from Kubo formula using the usual Hamiltonian Eq. (1) by several authors [1, 13–16] both for interband and intraband conductivity. We can calculate the optical conductivity for our Hamiltonian also following this approach. The eigenvectors for our Hamiltonian Eq. (2) is given by

$$|\vec{k}, +\rangle = \begin{pmatrix} \cos \frac{\theta}{2} \\ \sin \frac{\theta}{2} \end{pmatrix}, \quad |\vec{k}, -\rangle = \begin{pmatrix} \sin \frac{\theta}{2} \\ -\cos \frac{\theta}{2} \end{pmatrix} \quad (17)$$

for positive and negative energy states respectively. Here  $\theta$  is defined by  $A_{\vec{k}} = \lambda_{\vec{k}} \cos \theta$  and  $B_{\vec{k}} = \lambda_{\vec{k}} \sin \theta$ . Our objective is to study the variation of conductivity for different values of  $J$ . If we remain confined to  $\vec{k}$ -values for which  $\lambda_{\vec{k}} = \varepsilon_0$  then the real part of the diagonal conductivity for small frequency of an undoped material is given by

$$\text{Re}(\sigma_{\alpha\alpha}) \propto Q \quad \text{where} \quad Q = \sum_{\vec{k}} |\langle \vec{k}, + | j_\alpha | \vec{k}, - \rangle|^2 \quad (18)$$

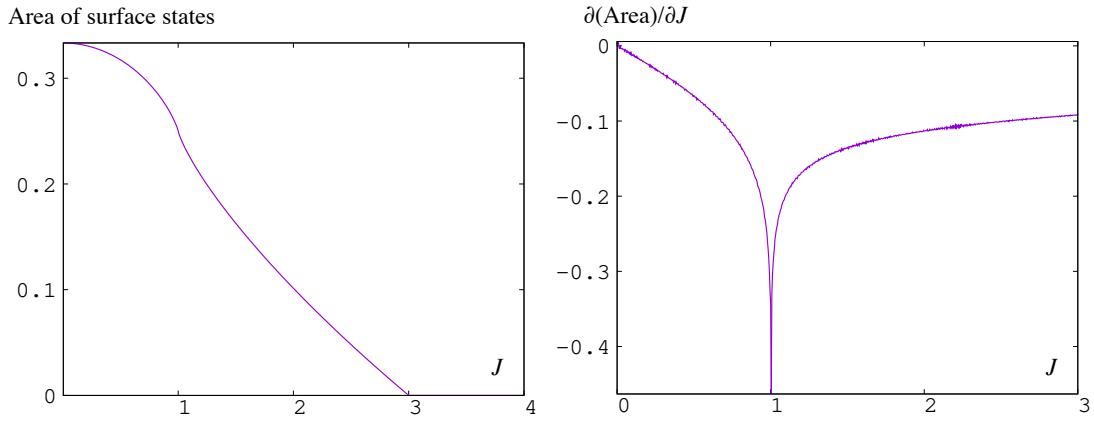


FIG. 7. The surface state area on  $k_x - k_y$  plane divided by the total area and its derivative are plotted with respect to  $J$

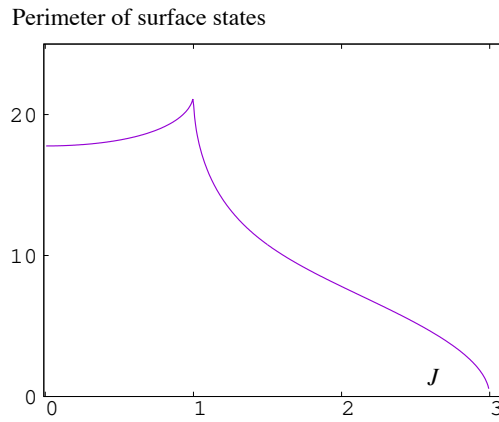


FIG. 8. The perimeter of the surface state area is plotted w.r.t  $J$

where  $\alpha = x, y, z$  and  $j_\alpha$  is the  $\alpha$ -th component of current density. Since the Hamiltonian is symmetric in  $x, y, z$ , the conductivity is the same for all values for  $\alpha$ . Since  $j_\alpha = -e\nabla_\alpha \mathcal{H}$ , one obtains

$$Q = \sum_{\vec{k}} \cos^2(k_x + \theta) \quad (19)$$

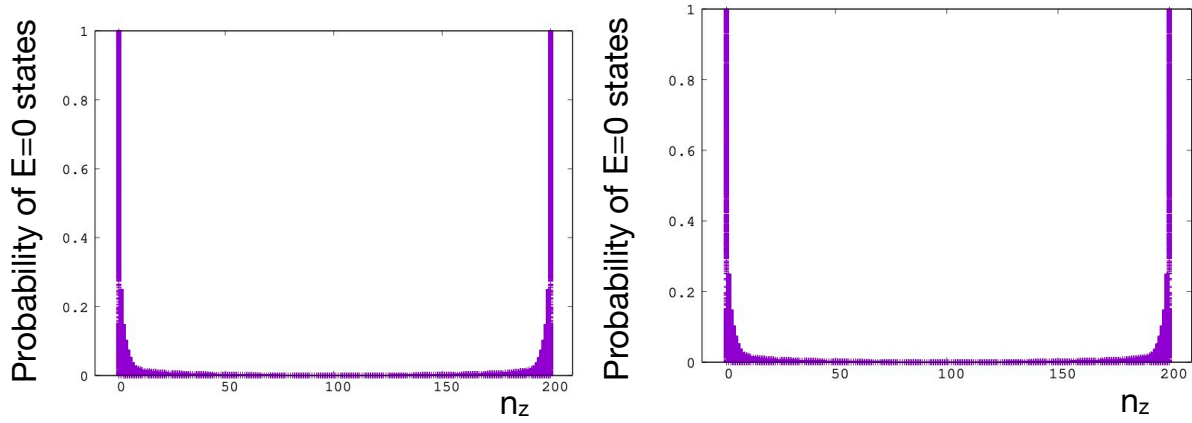


FIG. 9. The probability distribution of all the  $E = 0$  states vs  $N_z$  for  $J = 0.5$  (left) and  $J = 1.5$  (right)

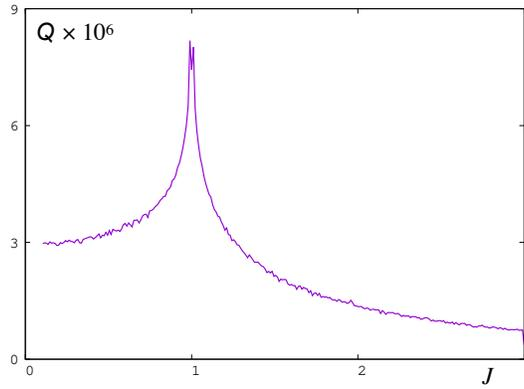


FIG. 10. Conductivity at a low frequency

The curve of conductivity as a function of  $J$  is similar to that of the length of nodal line as a function of  $J$ . It is generally believed that conductivity should be proportional to the length of the nodal line [17]

**Conclusion:** We study a spinless Hamiltonian

$$\mathcal{H} = \sum_{\vec{k}} [(J - \cos k_x - \cos k_y - \cos k_z) \sigma_z + (\sin k_x + \sin k_y + \sin k_z) \sigma_x] \quad (20)$$

and show that in addition to the well-known gapless to gapped transition at  $J = 3$ , there is another transition at  $J = 1$ . Both the transitions are marked by non-analyticities in the ground state energy vs  $J$  curve. Also, for the first gapless phase, namely for  $1 < J < 3$ , the nodes form one closed line lying in the first Brillouin zone without touching the zone-boundaries, while for the second (new) gapless phase  $J < 1$ , the nodal lines form a closed loop also, but now there are two such loops and each loop crosses the boundary surface of the first Brillouin zone. Furthermore, in the second phase (i) the number of zero energy surface states rise to a larger value (ii) the states with winding number 1 changes in topological character (iii) the electrical conductivity reaches a peak at the transition point  $J = 1$ . It seems interesting to analyse the behaviour of conductivity for this Hamiltonian and to look for materials which may be represented by this Hamiltonian.

---

\* protyush18@gmail.com

† subinaydasgupta@hri.res.in

- [1] A. A. Burkov, M. D. Hook and L. Balents, Phys. Rev. B **84**, 235126 (2011).
- [2] S. Shen, Topological Insulators: Dirac Equation in Condensed Matter (Springer, 2017).
- [3] N. P. Armitage, E. J. Mele, and A. Vishwanath, Rev. Mod. Phys. **90**, 015001 (2018).
- [4] M. Yang, W. Luo and W. Chen, Advances in Physics: X, **7**, 2065216 (2022).
- [5] G. Bian et.al., Nature Comm. **7**, 10556 (2016). DOI: 10.1038/ncomms10556.
- [6] Y. Oh, H. Min and Y. Kim, Phys. Rev. B **99**, 201110(R) (2019).
- [7] P. Nandi, S. Bhattacharyya and S. Dasgupta, Phys. Rev. Lett. **128**, 247201 (2022).
- [8] P. Nandi, S. Bhattacharyya and S. Dasgupta, arXiv: 2302.01795.
- [9] Ref [2], page 35.
- [10] Notes by Grushin,  
[https://grushingroup.cnrs.fr/wp-content/uploads/2021/05/intro\\_to\\_topo-1-1.pdf](https://grushingroup.cnrs.fr/wp-content/uploads/2021/05/intro_to_topo-1-1.pdf)
- [11] C. Chiu, J.C.Y. Teo, A.P. Schnyder, S. Ryu, Rev. Mod. Phys. **88**, 035005 (2016).
- [12] H. Shapourian, T.L. Hughes, Phys. Rev. B **93**, 075108 (2016).
- [13] S. Barati and S.H. Abedinpour, Phys. Rev. B **96**, 155150 (2017).
- [14] E.V. Gorbar, et. al., Phys. Rev. B **96**, 085130 (2017).
- [15] J.P. Carbotte, J. Phys. C **29**, 045301 (2017).
- [16] S. Ahn, E.J. Mele and H. Min, Phys. Rev. Lett **119**, 147402 (2017).
- [17] A.V. Pronin and M. Dressel, Physica Status Solidi B **258**, 2000027 (2021).
- [18] N.B. Kopnin, T.T. Heikkila, G.E. Volovik, Phys. Rev. B **83**, 220503(R) (2011)
- [19] H. Weng, Y. Liang, Q. Xu, R. Yu, Z. Fang, X. Dai, and Y. Kawazoe, Phys. Rev. B **92**(4), 045108 (2015)
- [20] . R. Yu, H. Weng, Z. Fang, X. Dai, and X. Hu, Phys. Rev. Lett. **115**(3), 036807 (2015)
- [21] Y. Kim, B. J. Wieder, C. L. Kane, and A. M. Rappe, Phys.Rev.Lett. **115**(3), 036806 (2015)

- [22] J. W. Rhim and Y. B. Kim, Phys. Rev. B **92**(4), 045126 (2015)
- [23] Z. Yan, P. W. Huang, and Z. Wang, Phys. Rev. B **93**(8), 085138 (2016)
- [24] Jun-Won Rhim and Yong Baek Kim, New J. Phys. **18** 043010 (2016)
- [25] Yejin Huh, Eun-Gook Moon, and Yong Baek Kim, Phys. Rev. B **93**, 035138 (2016)
- [26] Min-Xue Yang, Wei Luo, and Wei Chen, Advances in Physics: X, **7**:1, 2065216 (2022)